

1 Validation of optical coherence tomography as a tool to identify  
2 differentiation key drivers in 3D *in vitro* conjunctival models

3 Julian Schwebler<sup>1a,b</sup>, Fabiola Walz<sup>1a,b</sup>, Geraldine Beer<sup>a,b</sup>, Constantin Berger<sup>b</sup>, Olivier Thouvenin<sup>c</sup>,  
4 Djida Ghoubay<sup>c</sup>, Rodrigo Meléndez García<sup>c</sup>, Kate Grieve<sup>c</sup>, Christian Lotz<sup>\*b,a</sup>

5 <sup>a</sup> Department for Functional Materials in Medicine and Dentistry, University Hospital Würzburg,  
6 Würzburg, Bavaria, Germany

7 <sup>b</sup> Translational Center Regenerative Therapies TLC-RT, Fraunhofer Institute for Silicate Research  
8 ISC, Würzburg, Bavaria, Germany

9 <sup>c</sup> Institut de la Vision, Sorbonne Université, Hôpital National de la Vision des 15-20, INSERM,  
10 CNRS, F-75012 Paris, France

11 <sup>1</sup> Contributed equally to this study

12 \* Corresponding author: Christian Lotz

13 **Email:** christian.lotz@isc.fraunhofer.de

14 **Author Contributions:** J.S., F.W., C.B., and C.L. designed the study. J.S., F.W., G.B., D.G., O.T.,  
15 and R.M.G. performed the experiments. J.S., F.W., G.B., C.B., D.G., K.G, O.T., and R.M.G.  
16 analyzed data. C.L. and D.G. supervised the study and provided material. J.S. and F.W. wrote the  
17 manuscript. All authors revised the manuscript and agreed to the submitted version of the  
18 manuscript.

19 **Competing Interest Statement:** The authors declare no competing interests.

20 **Keywords:** Eye, Conjunctiva, Tissue Engineering, *in vitro* models, Optical Coherence  
21 Tomography

22

23

24

25

26

27

28

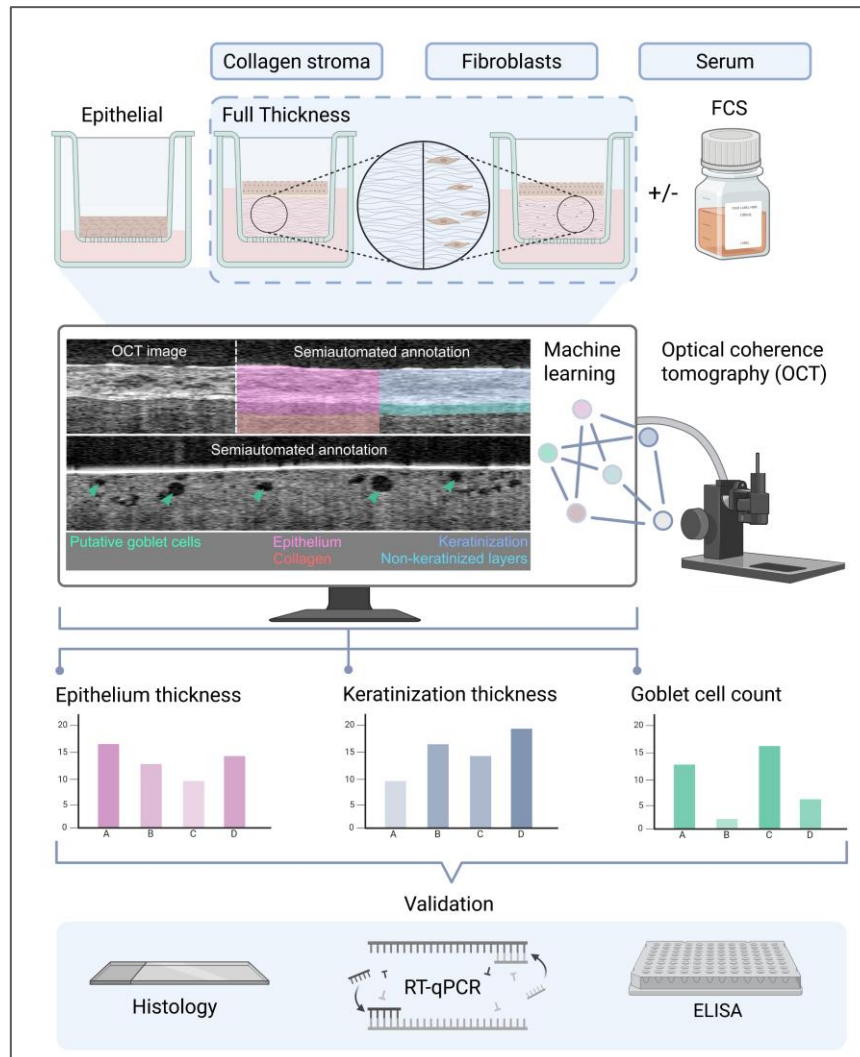
29

30

31

32

### 33 GRAPHICAL ABSTRACT



34

35

36

37

38

39

40

41

42 **ABSTRACT**

43 Conjunctival *in vitro* models present a valuable system to investigate conjunctival tissue  
44 homeostasis and pathologies. Combinations of collagen and fibroblasts as a stroma equivalent and  
45 the supplementation with serum have been reported to promote the differentiation of epithelial cells.  
46 However, how the individual factors affect differentiation of ocular surface cells is insufficiently  
47 understood. In this study, we analyzed the effect of serum concentration, a collagen matrix, and  
48 fibroblasts on conjunctival differentiation in a 3D *in vitro* model. For this purpose, we developed a  
49 computational analysis pipeline for the quantification of optical coherence tomography (OCT) data  
50 sets, allowing a time resolved, non-invasive assessment of conjunctiva epithelium differentiation,  
51 including goblet cell density. High-resolution dynamic full-field OCT (D-FFOCT) was employed to  
52 verify the identity of goblet cells. Conjunctival markers were further analyzed via histology, real-  
53 time quantitative PCR, and ELISA to confirm the data of the OCT analysis pipeline. We found that  
54 serum is required to induce epithelial differentiation while higher concentrations of 5 – 10% impaired  
55 epithelial development. The culture on a collagen matrix increased conjunctival markers upon  
56 stimulation with serum, while the co-culture with fibroblasts increased epithelial stratification.  
57 Increased serum concentration resulted in the increased occurrence of goblet cells of up to 20  
58 cells/mm<sup>2</sup>. Altogether, the complementary analyses confirmed the quantified OCT data.  
59 Summarized, we identified the combination of serum (3%), collagen, and fibroblasts as a condition  
60 resulting in the highest physiological resemblance. Altogether, our study emphasizes the need for  
61 fine-tuning of culture conditions for 3D *in vitro* models.

62

63 **SIGNIFICANCE STATEMENT**

64 Physiologically relevant *in vitro* conjunctiva models are essential for studying ocular surface  
65 homeostasis and disease. Our study refines 3D conjunctival culture conditions to more closely  
66 resemble native tissue by systematically identifying serum concentration, collagen scaffolds and  
67 fibroblasts as key drivers of epithelial differentiation. By applying non-invasive optical coherence  
68 tomography analysis, we enable longitudinal assessment of tissue maturation, addressing the need  
69 for non-destructive, repeatable tissue analysis.

70  
71  
72  
73  
74  
75  
76  
77  
78  
79  
80  
81  
82  
83  
84  
85  
86  
87  
88  
89  
90  
91

92 **MAIN TEXT**

93

94 **INTRODUCTION**

95

96 The conjunctiva plays a crucial role in maintaining the homeostasis of the tear film. Its secretion of  
97 mucus stabilizes the tear film by increasing the tear break-up time, while simultaneously protecting  
98 the ocular surface from pathogens<sup>1</sup>. The conjunctival epithelium consists of non-keratinized cells  
99 that express membrane-associated mucins, as well as specialized goblet cells, which secrete gel-  
100 forming and soluble mucins. The most prominent secreted mucin of conjunctival goblet cells is the  
101 gel-forming mucin 5AC (MUC5AC)<sup>2-4</sup>.

102 3D *in vitro* models of conjunctival tissue are used to investigate differentiation mechanisms of  
103 epithelial cells into goblet cells as well as to study diseases that affect the conjunctiva such as Dry  
104 Eye Disease or infections<sup>5-8</sup>. However, close physiological resemblance is needed for *in vitro*  
105 models to increase the transferability of the underlying research questions. In the case of the  
106 conjunctival epithelium, this includes a non-keratinized stratified epithelium with differentiated,  
107 mucin-expressing goblet cells. One prominent supplement used to generally trigger differentiation  
108 processes in *in vitro* models is human or bovine serum, typically at concentrations of 5 – 10%<sup>7-10</sup>.  
109 Furthermore, the co-culture of fibroblasts within an extracellular matrix (ECM) scaffold has  
110 previously been found to promote the differentiation of conjunctival epithelial cells<sup>8,11</sup>. Studies have  
111 shown that fibroblasts modulate epithelial cell behavior and enhance their differentiation<sup>12</sup>, while  
112 fibroblast growth factors (FGF) such as FGF2 and FGF10 promote goblet cell differentiation in the  
113 conjunctiva and intestine<sup>12-15</sup>. While these studies provided important insights into cell culture and  
114 differentiation processes, the specific effects of the individual variables – serum, ECM scaffolds,  
115 and fibroblasts – on the differentiation and stratification of epithelial cells is still unresolved.

116 A factor that is complicating research on *in vitro* models not only of the conjunctiva is the lack of  
117 reliable non-invasive imaging techniques. Histological and immunohistochemical staining present  
118 the gold standard for visualizing the tissue architecture in 3D *in vitro* models. However, fixation and  
119 labelling of the model require the destruction of the model, can introduce technical artifacts such  
120 as tissue shrinking, and capture only a snapshot of the model. Optical Coherence Tomography  
121 (OCT)<sup>16</sup> has emerged as a label-free, non-invasive imaging technique overcoming some of the  
122 disadvantages of label-dependent imaging techniques. OCT is widely used in ophthalmology to  
123 diagnose a variety of pathologies, such as macular degeneration and glaucoma<sup>16,17</sup>. Advancements  
124 of OCT have fueled its use in biomedical research such as cancer progression or kidney imaging<sup>18-</sup>  
125 <sup>20</sup>. While offering a limited resolution compared to microscope-based imaging techniques, OCT  
126 allows live-recording of *in vitro* models, which reduces the number of required models and allows  
127 to investigate spatiotemporal processes. Recently, dynamic full-field optical coherence tomography  
128 (D-FFOCT) module coupled to a commercial microscope equipped with a high-numerical aperture  
129 objective and a stage-top incubator has enabled imaging of retinal organoids<sup>21</sup> and other *in vitro*  
130 models<sup>22</sup> at subcellular resolution, revealing 3D structure with high resolution and intrinsic dynamic  
131 activity due to metabolic activity and cell function<sup>23-26</sup>.

132 In this study, we analyzed the effect of various fetal calf serum (FCS) concentrations, a collagen  
133 scaffold, and fibroblasts on conjunctival epithelial differentiation. We used OCT imaging to analyze  
134 3D conjunctiva models with respect to goblet cell number, keratinization, and epithelial thickness  
135 via OCT. Quantification of these parameters was achieved using the machine-learning-tool of the  
136 IMARIS software, providing a new approach of non-invasively evaluating 3D *in vitro* models on a  
137 qualitative and quantitative level. We found that all three factors have a distinct effect on  
138 conjunctival 3D *in vitro* models. In epithelial models, optimal FCS concentrations induced  
139 conjunctival differentiation, including an increased goblet cell number, and led to a disrupted  
140 stratification at higher concentrations. The use of a collagen matrix reduced keratinization and  
141 increased mucus production, while at the same time, it decreased the FCS concentration required  
142 to initially induce epithelial differentiation. Fibroblasts embedded in the collagen matrix led to better  
143 stratification of epithelial layers, while no significant goblet cell promoting effect was observed. The  
144 findings of this study give new insights into the effects and importance of culture conditions for

145 conjunctival tissue and can be used as orientation to achieve closer physiological resemblance in  
146 conjunctival *in vitro* models.

147

148

## 149 **RESULTS**

150

### 151 **Native conjunctiva and tissue models exhibit comparable morphology in OCT analysis**

152

153 Conventional methods to evaluate and characterize tissue models like histology are usually  
154 invasive, resulting in the destruction of the model. OCT has emerged as powerful non-invasive  
155 alternative, allowing the continuous monitoring and thus the observation of spatiotemporal  
156 processes within a single model<sup>20,24,27</sup>. Within this study, we employed OCT as a non-invasive  
157 analysis method for studying the effects of FCS concentrations and the presence of fibroblasts on  
158 conjunctival tissue model formation, with a particular focus on epithelial thickness, formation of  
159 unphysiological keratinization and goblet cell differentiation. To validate OCT as a suitable method  
160 to analyze epithelial conjunctival *in vitro* models, we initially used native human and porcine  
161 conjunctival tissue as a benchmark (Fig. 1A). OCT imaging of native tissue allowed the visualization  
162 of the conjunctival architecture, including a distinction between the epithelial and stromal  
163 compartment. Analysis of the FTConM revealed comparable structures with an observable  
164 demarcation of the epithelial layer. Dark, regularly shaped spots within the epithelium were visible  
165 in all three samples, which, according to their size and location putatively correlated to mucus-  
166 producing goblet cells. AB and PAS staining of the same porcine conjunctival tissue showed mucus  
167 filled cells, corroborating that the dark spots in the OCT indeed resemble goblet cells (Fig. 1B). To  
168 further validate our assumptions, we performed D-FFOCT on native human conjunctiva and the  
169 FTConM (Fig. 1C). In both samples, we detected cells with vacuoles visible as a dark inclusion that  
170 closely resemble the morphology of goblet cells.

171 Summarized, the data verify OCT as an adequate technique to visualize the conjunctival epithelium  
172 architecture including goblet cells, opening up the possibility to non-invasively monitor the  
173 differentiation and quality of conjunctival *in vitro* models.

174

### 175 **FCS induces differentiation and influences epithelial thickness in conjunctival epithelial 176 models**

177

178 Having verified the use of OCT for non-invasively visualizing relevant epithelial parameters, we  
179 next aimed to use this system to study the effect of varying FCS concentrations on the  
180 differentiation of conjunctival models. For this purpose, reconstructed human Conjunctival  
181 Epithelium (rhConE) models were cultured for 15 days and supplemented with increasing FCS  
182 concentrations ranging from 1 – 10%.

183 For the extraction of epithelial parameters from the recorded OCT datasets, we performed  
184 semiautomated image segmentation using the machine learning-assisted annotation tool of the  
185 Imaris software. This enabled the quantification of total epithelial layer thickness, non-keratinized  
186 layers, keratinization and goblet cell differentiation as demonstrated in Fig. 2A.

187 OCT imaging was performed on day 7, 12 and 15 to track the development of the rhConE in  
188 presence of various FCS concentrations (Fig. 2B). While no significant differences in total epithelial  
189 layer thickness were observed between varying FCS concentrations on day 7 epithelial thickness  
190 increased until day 15 in models cultured with FCS concentrations of 0 – 3% (Fig. 2C). Contrarily,  
191 higher FCS concentrations led to a slight reduction of epithelial layer thickness. OCT imaging  
192 further showed that the changes in epithelial thickness resulted primarily from variations in  
193 keratinization, while the thickness of the non-keratinized layers remained unchanged across all  
194 conditions and time points. Prominent keratinization was observed for FCS concentrations of 0 –  
195 2% on day 15. Interestingly, further increase of FCS concentrations resulted in a reduction of  
196 keratinization, with 3% and 4% FCS showing reduced and 5% and 10% FCS exhibiting strongly

197 diminished keratinization. On day 12, putative goblet cells started to appear in rhConE exposed to  
198 3% FCS or higher, with a maximum number of approximately 10 counts/mm<sup>2</sup> at 4 – 5% FCS.  
199 To validate the findings made by quantitative OCT imaging, H&E staining was performed on day  
200 15, as well as AB and PAS staining to stain mucus (Fig. 3). RhConE showed a multi-layered  
201 epithelium with a thick keratinization at 0 – 2% FCS supplementation. While PAS staining  
202 intensified from 0 – 2%, no goblet cells were observed. In correlation with the occurrence of dark  
203 spots in the OCT, AB and PAS-positive goblet cells with a cup-like structure were detectable at 3  
204 – 10% FCS. Histological stainings confirmed the reduction of keratinization and epithelial thickness  
205 measured in OCT-analyses with increasing FCS concentration. At FCS concentrations of ≥ 4%, we  
206 observed a decreased tissue stratification with flattened basal cells, indicating a negative influence  
207 of high FCS concentrations on the epithelial organization of rhConE.  
208 Next, we analyzed the gene expression of the conjunctival markers to study the dose-dependent  
209 effect of FCS on conjunctival differentiation. *KRT13* expression was significantly elevated at 1%  
210 and 2% FCS compared to 0% FCS, with fold changes of  $240 \pm 105$  and  $506 \pm 72$ , respectively (Fig.  
211 4A). At ≥ 3% FCS, *KRT13* expression was elevated up to 79-fold compared to rhConE cultured  
212 without FCS, but significantly less increased compared to 2% FCS. *KRT19* expression increased  
213 in a dose-dependent manner from 0 – 3% and remained constant at ≥ 3% FCS at approximately  
214 1200- to 1500-fold change compared to 0% FCS. In contrast to *KRT19* expression, *LORICRIN*, a  
215 marker for the cornified envelope<sup>28</sup>, decreased with increasing FCS concentrations and showed a  
216 significant reduction at ≥ 3% compared to the FCS-free condition, indicating a diminishing effect of  
217 elevating FCS concentrations on keratinization and supporting the findings made by the OCT data  
218 quantification.  
219 Immunofluorescence staining confirmed the gene expression data (Fig. 4B). While the signal of  
220 CK13 peaked at 3% FCS supplementation, CK19 staining appeared stronger with increasing FCS  
221 concentration. Loricrin staining was detectable in the upper region of the epithelial layers in rhConE  
222 supplemented with 0 – 2% FCS, but not detectable at 3 – 10% FCS supplementation, proving a  
223 keratinization-inhibiting effect of increasing FCS concentrations. Collagen IV (Col IV), stained for  
224 the comparison with FTConM, was not detectable in rhConE.  
225 To verify the beneficial effect of increasing FCS concentrations on the number of goblet cells  
226 detected by OCT and histological stainings, gene expression of the membrane-associated mucins  
227 *MUC1*, *MUC4*, and *MUC16* was analyzed (Fig. 4C). The expression of all three mucins increased  
228 with higher FCS concentration. A significant elevation of *MUC4* expression was measured in  
229 models cultured with 3% FCS, while *MUC1* and *MUC16* transcript levels were significantly  
230 increased at 4% FCS and 10% FCS, respectively. Furthermore, the secretion of MUC5AC was  
231 measured via ELISA (Fig. 4D). The highest MUC5AC secretion was observed at 3% FCS and  
232 showed lower concentrations with increasing FCS supplementation, indicating that higher FCS  
233 concentrations were detrimental for MUC5AC secretion of goblet cells.  
234 Summarized, the acquired data demonstrate that increasing FCS concentrations prevent  
235 keratinization and increase the number of goblet cells of rhConE, while exposure to ≥ 4% FCS  
236 impairs a regular epithelial stratification. Importantly, the conducted experiments verified  
237 quantitative OCT as an adequate method to assess epithelial architecture and goblet cell number.

### 238 239 **The connective tissue equivalent promotes differentiation and stratification in conjunctival** 240 ***in vitro* models**

241  
242 As a next step, we analyzed whether the addition of a connective tissue equivalent promotes  
243 epithelial cell differentiation and improves the structure of conjunctival models. Conjunctival  
244 epithelial cells were cultured on a compressed collagen matrix without (w/o Fib.) or with (w/ Fib.)  
245 embedded conjunctival fibroblasts. To investigate the effect of FCS on epithelial formation in the  
246 presence of fibroblasts, both conditions were subjected to 0 – 3% FCS supplementation.  
247 OCT-images of FTConM were analyzed using machine learning-assisted segmentation, as  
248 performed for rhConE (Fig. 5A). Total epithelial thickness, non-keratinized layers, keratinization  
249 and goblet cells could be identified as distinguishable structures (Fig. 5B). Quantitative analyses  
250 revealed an increasing epithelial thickness from day 7 ( $79 \pm 7 \mu\text{m}$ ) to day 15 ( $155 \pm 19 \mu\text{m}$ ),

251 regardless of FCS concentration (Fig. 5C). In contrast to the rhConE models, keratinization of the  
252 epithelium was prevented at lower FCS concentrations, and the total epithelial thickness was not  
253 reduced at higher FCS concentrations. While at 0 – 1% FCS the increase of the total epithelial  
254 thickness resulted almost exclusively from a thickening of the keratinized layer, FTConM exposed  
255 to 2 – 3% FCS remained non-keratinized and exhibited an increased height of the non-keratinized  
256 epithelial layers. Interestingly, models cultured with fibroblasts showed fewer epithelial layers at  
257 d15 compared to models cultured without. On the other hand, models cultured with fibroblasts  
258 showed a more defined stratification especially at higher FCS concentrations, with a clear  
259 demarcation between epithelium and collagen. Goblet cells started to appear in models cultured  
260 with 2% FCS and, more frequently, with 3% FCS. In both cases, goblet cell frequency increased  
261 over time.

262 Histological analysis confirmed a reduced keratinization of models with and without fibroblasts  
263 cultured at  $\geq 2\%$  FCS (Fig. 6). PAS staining gradually intensified from 0% to 3% FCS. Goblet cells  
264 were present in FTConM treated with 2% and 3% FCS. In FTConM cultured without fibroblasts, we  
265 observed an invasive behavior of epithelial cells into the collagen scaffold. This effect was more  
266 prominent with increasing FCS concentrations compared to 0% FCS, where no invasion was  
267 detected at all. In models cultured with conjunctival fibroblasts, no invasive epithelial cells were  
268 observed. FTConM exposed to 3% FCS exhibited a more distinct basal layer of epithelial cells  
269 when cultured with fibroblasts than without. Overall, the stratification of epithelial layers was more  
270 structured in models cultured with fibroblasts and higher FCS concentrations, while this was not  
271 the case for models without FCS supplementation, suggesting that conjunctival fibroblasts secrete  
272 factors that promote epithelial stratification.

273 Gene expression analysis revealed a significant increase of *KRT13* expression at 2% and 3% FCS,  
274 and *KRT19* at 3% FCS, both with and without fibroblasts (Fig 7A). *LORICRIN* was significantly  
275 reduced at 3% FCS for both conditions. At 2% FCS, the expression of *KRT13* was significantly  
276 higher in models cultured without fibroblasts which was not the case for other FCS concentrations.  
277 No significant difference in the expression of *KRT19* and *LORICRIN* was observed between models  
278 cultured with and without fibroblasts.

279 Immunofluorescent staining of FTConM with and without fibroblasts cultured without FCS showed  
280 no CK13 and CK19 staining, whereas Loricrin was detectable in both conditions (Fig. 7B). CK13  
281 and CK19 were detectable in FTConM treated with 2% FCS, with an increased signal intensity at  
282 3% FCS, both with and without fibroblasts. The combination of fibroblasts and FCS further resulted  
283 in the secretion of the basement membrane protein Col IV. In FTConM without fibroblasts, Col IV  
284 was absent at 0 – 2% FCS while single spots were stained at 3%. In FTConM cultured with  
285 fibroblasts, small spots of Col IV were detected underneath the epithelial basal layer at 1% FCS,  
286 with an increased signal intensity at 2%. With 3% FCS, a defined basement layer of Col IV could  
287 be detected underneath the epithelium. In line with the increased number of goblet cells revealed  
288 by quantitative OCT, the number of transcripts encoding for the membrane associated mucins  
289 *MUC1*, *MUC4*, and *MUC16* was increased by FCS in a dose-dependent manner (Fig. 7C).  
290 Similarly, FCS administration resulted in an elevated secretion of the secretory mucin MUC5AC  
291 (Fig. 7D). The inclusion of fibroblasts had no effect on mucin expression or secretion.

292 Taken together, the data confirm that FCS concentrations of 2% and 3% resulted in a more  
293 differentiated, non-keratinized epithelium with a thicker epithelial layer and a higher frequency of  
294 goblet cells, while the combination with fibroblasts improved epithelial stratification and Col IV  
295 deposition.

296  
297

## 298 DISCUSSION

299

300 Previously, we demonstrated that the incorporation of a connective tissue equivalent promotes the  
301 differentiation of our conjunctival *in vitro* model towards a physiological morphology<sup>11</sup>. In this study,  
302 we analyzed the individual components of the connective tissue equivalent regarding their effects  
303 on conjunctival differentiation. We found distinct effects for FCS, collagen, and fibroblasts on  
304 epithelial differentiation and stratification. Previous studies demonstrated the promoting properties

305 of fibroblasts and collagen on mucosal differentiation<sup>8,29</sup>. While these studies gave important  
306 insights on conjunctival differentiation, FCS was used in their culture medium, making it difficult to  
307 determine the effect of individual factors. In general, serum is an important supplement for the  
308 culture of various cell types and is widely used at concentrations ranging from 5 – 10%<sup>7-10</sup>. In our  
309 study, we show that these concentrations are not ideal for the culture of conjunctival 3D *in vitro*  
310 models, as serum concentrations of  $\geq 5\%$  prevented the growth of a multi-layered and stratified  
311 epithelium. However, in both rhConE and FTConM, FCS was needed to initially induce mucous  
312 differentiation and shift conjunctival epithelial cells from a pathological keratinized state toward a  
313 more natural conjunctival phenotype. Of the numerous factors contained in FCS, retinoic acid  
314 (RA)<sup>30</sup> and Interleukin-13 (IL-13)<sup>31</sup> present interesting candidates for mediating the observed  
315 effects. In conjunctival organoids, RA has recently been shown to promote differentiation while IL-  
316 13 is known to enhance goblet cells and mucus expression in mucosal tissue<sup>32-35</sup>.  
317 The FCS-driven differentiation could also explain the impairment of epithelial stratification observed  
318 at higher FCS concentrations. Since cell proliferation decreases with increased differentiation<sup>36</sup>,  
319 factors in FCS that cause differentiation may in turn reduce cell proliferation, impairing stratification  
320 due to a reduced cell mass. In the light of these findings, fine tuning of FCS or the addition of a  
321 defined growth factor supplementation emerges as a vital task to ensure the formation of  
322 conjunctival *in vitro* models that properly mimic an *in vivo* histology.  
323 The comparison of rhConE and FTConM showed that besides FCS, collagen had a positive effect  
324 on epithelial cells. In detail, we demonstrate in our study that the use of a collagen matrix did not  
325 induce differentiation alone but reduced the FCS concentration needed to achieve a conjunctival  
326 phenotype, determined by the reduction of keratinization, retainment of a multi-layered epithelium,  
327 and induction of goblet cells at lower concentrations. In this way the use of collagen also  
328 circumvents the negative effects caused by high serum concentrations. Zhou et al. showed that  
329 Col I promoted the expression of MUC5AC<sup>37</sup> which we could confirm in our study via the  
330 comparison of rhConE and FTConM in a MUC5AC ELISA. These beneficial effects of collagen  
331 might originate from its lower stiffness compared to cell culture inserts, as well as the interaction  
332 between collagen proteins and integrins on epithelial cells, which can induce intracellular  
333 downstream signaling<sup>38,39</sup>.  
334 A clear demarcation between the stroma equivalent and the basal layer was lost with increasing  
335 FCS concentrations and epithelial cells showed an invasive behavior. Serum, particularly the  
336 contained factors TGF- $\beta$  and EGF, have been shown to promote epithelial-mesenchymal transition  
337 (EMT) in epithelial cells<sup>40,41</sup>, characterized by a transition towards more invasive behavior, cell  
338 migration and a reduction of cell-cell adhesion markers like E-cadherin<sup>40</sup>. Epithelial invasion was  
339 mitigated by the inclusion of fibroblasts into the collagen scaffold. The addition of fibroblasts further  
340 resulted in a clear demarcation at all FCS concentrations and an increased stratification of the  
341 epithelial layers. The interaction of epithelial and stromal cells is an important factor, especially due  
342 to the expression of growth factors and matrix remodeling. Mesenchymal cells express FGFs, of  
343 which FGF2, FGF7, and FGF10 promote proliferation<sup>42-45</sup>. However, to our knowledge little is  
344 known about the spectrum of secreted growth factors by conjunctival fibroblasts. Thus, future  
345 investigations could elucidate which specific interactions contributed to the retainment of epithelial  
346 architecture. Furthermore, fibroblasts are known to change and remodel their ECM environment,  
347 for example by the secretion of matrix metalloproteinases (MMPs)<sup>46-49</sup>, leading to a contraction of  
348 collagen which results in a denser, more structured matrix<sup>50</sup>. By remodeling the collagen scaffold,  
349 fibroblasts therefore possibly prevented epithelial invasion in a mechanical manner. We also  
350 detected Col IV, an essential component of basement membranes<sup>51,52</sup>, at the interface of scaffold  
351 and epithelium which was most defined in the presence of fibroblasts at 2% and 3% FCS  
352 supplementation. This might result from the activation and enhanced collagen deposition of  
353 fibroblast induced by FCS<sup>53</sup>. As a functional basement membrane is important for the regulation of  
354 cell migration and tissue organization<sup>51</sup>, the presence of a developing basement membrane at the  
355 scaffold-epithelium interface may have contributed to the improved epithelial stratification observed  
356 in our model. Regarding mucus expression, the effect of fibroblasts is unclear in literature. Tsai et  
357 al. demonstrated that conjunctival fibroblasts promote mucus producing cells<sup>8</sup> while Massaro et al.  
358 showed in an intestinal co-culture model of fibroblasts and epithelial cells a fibroblast-dependent

359 reduction of gel-forming mucin expression<sup>54</sup>. Interestingly, further studies show that Col IV reduces  
360 MUC5AC in airway cells<sup>55,56</sup>. As we observed no effect of fibroblasts on mucus production, further  
361 investigation is necessary in the future to determine when fibroblasts influence its expression and  
362 whether the presence of Col IV has a respective effect in 3D *in vitro* models.  
363 Within this study, we used OCT to monitor the tissue development over time and to analyze the  
364 aforementioned cellular and structural effects. We were able to distinguish model structures,  
365 including keratinized and non-keratinized epithelia, as well as the membrane or the stroma  
366 equivalent. Effects of culture conditions observed in OCT were supported by RT-qPCR, histological  
367 analyses, and ELISA, confirming the validity of this approach. OCT is widely applied for  
368 ophthalmologic diagnostics, such as for retinal and ocular surface imaging<sup>57</sup>. Recently, OCT is  
369 increasingly used in tissue engineering and *in vitro* applications<sup>24,58,59</sup>. Conventional OCT enabled  
370 quantification of vacuoles, which with a very high level of confidence correspond to individual goblet  
371 cells. A study by Aguirre et al. confirms the observation of goblet cells as distinct, non-scattering  
372 inclusions in optical coherence microscopy images<sup>60</sup>. Although intensity-based image  
373 segmentation allowed reliable detection of dark spots within the epithelium, unambiguous  
374 identification of goblet cells was complicated by the presence of gaps in the epithelium, which likely  
375 result from reduced cell-cell-adhesion and similarly present as dark areas. Inclusion of defined post-  
376 segmentation object filtering nevertheless enabled a representative assessment of goblet cell  
377 numbers and the differentiation status, supported by the strong correlation between OCT-based  
378 quantification and the data from RT-qPCR, ELISA as well as histological analyses. Future possible  
379 improvements to maximize the read-out quality of goblet cells include combinatorial approaches,  
380 such as additional D-FFOCT images to identify cell structures around vacuoles, as well as dynamic  
381 microscopic OCT, which has previously been shown to allow the identification of individual cells<sup>61</sup>.  
382 Furthermore, Kim et al. showed the use of moxifloxacin to label goblet cells non-invasively, which  
383 could also be used as a complementary method<sup>62</sup>.  
384 Nevertheless, we show that OCT is a suitable method for non-invasive monitoring of conjunctival  
385 *in vitro* tissue, as it captures relevant structural features and does not rely on the administration of  
386 any substances, enabling a quick evaluation of generated models with high quality. A future step  
387 in goblet cell analysis could be the distinction between mucus filled and empty cells. This could  
388 enable easier investigation of conjunctival pathologies that affect mucin secretion such as dry eye  
389 disease or allergic conjunctivitis<sup>61,63,64</sup>.  
390 Summarized, we used qualitative and quantitative OCT techniques in combination with gene and  
391 protein expression analyses to show the individual effects of FCS concentrations, a collagen matrix,  
392 and co-cultured fibroblasts on conjunctival differentiation and stratification. Overall, the highest  
393 physiological resemblance was achieved by the combination of all three factors with 3% FCS  
394 supplementation. This could pave the way for more predictive and relevant *in vitro* models as well  
395 as for new non-invasive analysis tools to research differentiation processes.

396  
397

## 398 **MATERIALS AND METHODS**

399  
400

### 400 **Conjunctival tissue**

401

402 The experiments performed in this study followed the Declaration of Helsinki. The local ethics  
403 committees (IRB of the Medical Faculty of the University of Wuerzburg; approval numbers 187/17,  
404 195/13, 82/10 and 2018-280\_5-dvh and French Society of Ophthalmology, approval number IRB  
405 00008855) approved the use of human material. Conjunctival biopsies were obtained from adult  
406 patients of the Department of Ophthalmology, University Hospital Würzburg with informed consent  
407 or from enucleated eyes for corneal graft preparation from deceased organ donors, after informed  
408 consent from their relatives. The biopsies used for this study did not show other ocular pathologies  
409 that affect the conjunctiva such as pemphigoid, pterygium, or significant inflammation. All biopsies  
410 were anonymized and assigned to a number.  
411 Porcine tissue was kindly provided by a local slaughterhouse and used immediately upon  
412 obtainment.

## 413 **Isolation and culture of primary human conjunctival cells**

414

415 The isolation of primary human conjunctival epithelial cells and fibroblasts as well as the generation  
416 of reconstructed human Conjunctival Epithelium models (rhConE) and Full Thickness Conjunctiva  
417 Models (FTConM) was performed as previously described<sup>11</sup>. RhConE were cultured in Pro10-  
418 Medium (PromoCell Keratinocyte Growth Medium 2 + Supplement Mix (PromoCell, Heidelberg,  
419 Germany) + 1% Penicillin/Streptomycin (Sigma Aldrich, Darmstadt, Germany) + 1.5 mM CaCl<sub>2</sub>  
420 (Sigma Aldrich, Darmstadt, Germany) + 73 µg/mL Ascorbic acid-2-phosphate (Sigma Aldrich,  
421 Darmstadt, Germany) + 10 ng/mL Keratinocyte Growth Factor (KGF, PeproTech Proteins, Thermo  
422 Fisher, Waltham, USA) + 10% FibroLife medium (without supplement LifeFactor, Epidermal Growth  
423 Factor, Transforming Growth Factor-β, Gentamicin, and Amphotericin, Lifeline Cell Technology,  
424 San Diego, USA)). Depending on the experiment, FCS was added at concentrations of 1 – 5% or  
425 10%. Epithelial cells were used in passage (p) 3 for model generation while fibroblasts were used  
426 in p5.

427

## 428 **Quantitative Optical Coherence Tomography**

429

430 Optical coherence tomography was used as a non-invasive method to observe and quantify the  
431 structural development of the *in vitro* models. To acquire OCT image data, a commercial spectral-  
432 domain OCT (SD-OCT) Ganymede system (Thorlabs GmbH, Bergkirchen, Germany), equipped  
433 with a GAN621 base unit and an OCT-LK3-BB objective, was used. The light source has a nominal  
434 center wavelength of 900 nm and an axial resolution of 3 µm.

435 On day 7, 12 and 15, volumetric OCT-scans were acquired for each model, with an X-Y scan area  
436 of 5 x 2 mm<sup>2</sup>, a pixel size of 10 x 10 µm<sup>2</sup> and a 25 kHz A-Scan rate.

437 To analyze the volumetric image data in terms of quantification of epithelial thickness, keratinization  
438 and number of goblet cells, the respective structures were annotated using machine learning  
439 segmentation in Imaris (Version 10.2.0, Bitplane AG, Zurich, Switzerland). For quantification of the  
440 epithelial layers and keratinization, the volume of the annotated structure was divided by the scan  
441 area to obtain the average thickness of each layer per scan. The number of goblet cells was  
442 approximated by counting dark spots within the epithelium, with a diameter of 20 – 60 µm and a  
443 sphericity greater than 0.8.

444

## 445 **Dynamic Full-Field Optical Coherence Tomography**

446

447 Native human conjunctiva and FTConM were obtained or generated as previously described<sup>11</sup>.  
448 Samples were mounted in black, flat-bottom glass 24-well plates compatible with cell culture and  
449 microscopy (Cellvis, P24-1.5H-N) and placed in a stage-top incubator (H201-K-FRAME, H201-  
450 MW-HOLDER, and OBJ-COLLAR-2532; Okolab). Prior to imaging, samples were equilibrated in  
451 the incubator to stabilize temperature and CO<sub>2</sub> concentration (37 °C, 5% CO<sub>2</sub>). Dynamic, non-  
452 invasive, label-free live-cell imaging was performed using a custom D-FFOCT module coupled to  
453 a commercial microscope, as previously described<sup>22</sup>. Volumetric acquisitions were performed with  
454 sufficient lateral and axial coverage to resolve goblet cell morphology. Image and volume  
455 reconstruction was carried out using ImageJ software.

456

## 457 **Histology**

458

459 Native tissue as well as conjunctival models were fixed in Rotifix® (Carl Roth, Germany) for 2 h at  
460 room temperature (RT) and embedded in paraffin. Sections of 3.5 µm were prepared from paraffin  
461 blocks and used for staining. For histological staining, sections were dewaxed and rehydrated  
462 before staining with Hematoxylin&Eosin (H&E; Morphisto, Offenbach am Main, Germany), Alcian  
463 blue (AB; Morphisto, Offenbach am Main, Germany), and Periodic acid Schiff (PAS; Carl Roth  
464 GmbH + Co. KG, Karlsruhe, Germany) according to the manufacturer's guidelines. Stained  
465 sections were dehydrated and mounted with Entellan (Merck, Darmstadt, Germany).

466 For immunofluorescence, paraffin sections were deparaffinized and rehydrated. Next, heat  
467 mediated antigen retrieval was performed by incubation in citrate buffer pH 6 at 95 °C for 20 min.  
468 Subsequently, sections were blocked in 5% Bovine Serum Albumin (BSA, Carl Roth, Karlsruhe,  
469 Germany) for 20 min. Primary antibodies were applied over night at 4 °C. On the next day, sections  
470 were washed three times in washing buffer (PBS + 0.5% Tween-20, VWR, Radnor, PA, USA).  
471 Secondary antibodies were applied for 1 h at RT. Subsequently, the slides were washed three  
472 times in washing buffer and mounted with FluoroMount™ containing DAPI (Invitrogen, Carlsbad,  
473 CA, USA). The following primary antibodies were used: Cytokeratin 13 (Dilution 1:200, sc-390982,  
474 Santa Cruz Biotechnology, Dallas, TX, USA), Cytokeratin 19 (Dilution 1:200, ab7754, Abcam,  
475 Cambridge, UK), Collagen IV (Dilution 1:500, ab6586, Abcam, Cambridge, UK), and Loricrin  
476 (Dilution 1:500, ab85679, Abcam, Cambridge, UK). The following secondary antibodies were used:  
477 AlexaFluor® 555, 647 (dilution 1:400, LifeTechnologies, Carlsbad, CA, USA).

478

#### 479 **Reverse transcription Real Time quantitative PCR (RT-qPCR)**

480

481 Conjunctival models were lysed in 350 µl TRK lysis buffer (VWR International, Radnor,  
482 Pennsylvania, USA) supplemented with 20 µl/mL β-Mercaptoethanol and homogenized in a Tissue  
483 lyser (Qiagen, Hilden, Germany). Total RNA was isolated using the peqGold Total RNA Kit (VWR  
484 International, Radnor, Pennsylvania, USA). 500 ng of RNA was transcribed into cDNA using the  
485 iScript™ cDNA Synthesis Kit (Bio-Rad, Hercules, California, USA). RT-qPCR was performed using  
486 the SsoAdvanced Universal SYBR Green Supermix (Bio-Rad, Hercules, California, USA) and the  
487 QuantStudio™ 7 Flex system (Thermo Fisher, Waltham, USA). All runs were performed with 60 °C  
488 annealing temperature. Gene expression was calculated using the  $\Delta\Delta CT$ -method with 18s as  
489 housekeeper reference. Primer sequences (Eurofins Scientific, Luxembourg) were used as stated  
490 in Table 1.

491

#### 492 **ELISA**

493

494 The concentration of secreted MUC5AC was assessed via ELISA of cell culture supernatant  
495 samples from day 15 of model culture with fresh culture medium as a control. Samples were stored  
496 at -80°C until further use. The assays were performed according to the manufacturer's instructions  
497 (Human MUC5AC ELISA Kit (colorimetric), bio-technie, Minneapolis, MN, USA). Colorimetric  
498 measurements were performed on a TECAN Spark system (Tecan Group, Männedorf,  
499 Switzerland). MUC5AC concentrations were determined from a standard curve.

500

#### 501 **Statistical analysis**

502

503 Graphpad Prism 10 software (Graphpad Software Inc., La Jolla, CA, USA) was used for statistical  
504 analyses. Data sets were tested for normality via Shapiro-Wilk tests. Quantitative OCT analysis  
505 was evaluated via Two-way ANOVA. For RT-qPCR analyses, normally distributed data was  
506 analyzed via parametric One-way ANOVA with Tukey's multiple comparisons test, while non-  
507 normally distributed data sets were analyzed via Kruskal-Wallis tests with Dunn's multiple  
508 comparisons test. Values of  $p < 0.05$  were considered significant.

509

510

#### 511 **ACKNOWLEDGMENTS**

512

513 The authors thank the Department of Ophthalmology of the University Hospital Würzburg for kindly  
514 providing biological material used in this study. The authors further thank Barbara Bayer, Annika  
515 Baumann, and Alevtina Höchner for their excellent technical support. This study was funded by the  
516 European Union within the frame of the Horizon Europe project: HORIZON-HLTH-2023-TOOL-05-  
517 01 under grant agreement No.101137315.

518

519

## 520 REFERENCES

- 521 1. Chang AY, Purt B. *Biochemistry, Tear Film*. StatPearls. 2025.
- 522 2. Hori Y. Secreted Mucins on the Ocular Surface. *Invest Ophthalmol Vis Sci*. Nov 1  
523 2018;59(14):Des151-des156. doi:10.1167/iovs.17-23623
- 524 3. Mantelli F, Argüeso P. Functions of ocular surface mucins in health and disease. *Curr Opin*  
525 *Allergy Clin Immunol*. Oct 2008;8(5):477-83. doi:10.1097/ACI.0b013e32830e6b04
- 526 4. Shumway CL, Motlagh M, Wade M. Anatomy, Head and Neck, Eye Conjunctiva. *StatPearls*.  
527 2025.
- 528 5. Bannier-Hélaouët M, Korving J, Ma Z, et al. Human conjunctiva organoids to study ocular  
529 surface homeostasis and disease. *Cell Stem Cell*. Feb 1 2024;31(2):227-243.e12.  
530 doi:10.1016/j.stem.2023.12.008
- 531 6. Domínguez-López A, Blanco-Vázquez M, Calderón-García A, et al. Analysis of the mucosal  
532 chemokines CCL28, CXCL14, and CXCL17 in dry eye disease: An *in vitro* and clinical  
533 investigation. *Exp Eye Res*. Apr 2024;241:109854. doi:10.1016/j.exer.2024.109854
- 534 7. García-Posadas L, Soriano-Romaní L, López-García A, Diebold Y. An engineered human  
535 conjunctival-like tissue to study ocular surface inflammatory diseases. *PLOS ONE*.  
536 2017;12(3):e0171099. doi:10.1371/journal.pone.0171099
- 537 8. Tsai RJ, Ho YS, Chen JK. The effects of fibroblasts on the growth and differentiation of human  
538 bulbar conjunctival epithelial cells in an *in vitro* conjunctival equivalent. *Invest Ophthalmol Vis Sci*.  
539 May 1994;35(6):2865-75.
- 540 9. Lu Q, Yin H, Grant MP, Elisseeff JH. An *In vitro* Model for the Ocular Surface and Tear Film  
541 System. *Sci Rep*. Jul 21 2017;7(1):6163. doi:10.1038/s41598-017-06369-8
- 542 10. Warcoin E, Clouzeau C, Roubeix C, et al. Hyperosmolarity and Benzalkonium Chloride  
543 Differently Stimulate Inflammatory Markers in Conjunctiva-Derived Epithelial Cells *in vitro*.  
544 *Ophthalmic Res*. 2017;58(1):40-48. doi:10.1159/000448117
- 545 11. Schwebler J, Fey C, Kampik D, Lotz C. Full thickness 3D *in vitro* conjunctiva model enables  
546 goblet cell differentiation. *Scientific Reports*. 2023/07/28 2023;13(1):12261. doi:10.1038/s41598-  
547 023-38927-8
- 548 12. Massaro A, Villegas Novoa C, Wang Y, Allbritton NL. Fibroblasts modulate epithelial cell  
549 behavior within the proliferative niche and differentiated cell zone within a human colonic crypt  
550 model. *Front Bioeng Biotechnol*. 2024;12:1506976. doi:10.3389/fbioe.2024.1506976
- 551 13. Al Alam D, Danopoulos S, Schall K, et al. Fibroblast growth factor 10 alters the balance  
552 between goblet and Paneth cells in the adult mouse small intestine. *American Journal of*  
553 *Physiology-Gastrointestinal and Liver Physiology*. 2015;308(8):G678-G690.  
554 doi:10.1152/ajpgi.00158.2014
- 555 14. Ma M, Zhang Z, Niu W, Zheng W, Kelimu J, Ke B. Fibroblast growth factor 10 upregulates the  
556 expression of mucins in rat conjunctival epithelial cells. *Mol Vis*. 2011;17:2789-97.
- 557 15. Yokoo S, Yamagami S. Goblet Cell Differentiation Potential in Human Corneal Limbal  
558 Epithelial Progenitor Cells *In vitro*. *Investigative Ophthalmology & Visual Science*.  
559 2020;61(12):27-27. doi:10.1167/iovs.61.12.27
- 560 16. Huang D, Swanson EA, Lin CP, et al. Optical Coherence Tomography. *Science*.  
561 1991;254(5035):1178-1181. doi:doi:10.1126/science.1957169
- 562 17. Schuman JS, Hee MR, Arya AV, et al. Optical coherence tomography: a new tool for  
563 glaucoma diagnosis. *Curr Opin Ophthalmol*. Apr 1995;6(2):89-95. doi:10.1097/00055735-  
564 199504000-00014
- 565 18. Burhan S, Göb M, Pieper M, et al. Label-free volumetric imaging of porcine kidney tissue over  
566 extended areas using dynamic MHz-OCT. *Scientific Reports*. 2025/09/12 2025;15(1):32426.  
567 doi:10.1038/s41598-025-15032-6
- 568 19. Mulligan JA, Ling L, Leartprapun N, Fischbach C, Adie SG. Computational 4D-OCM for label-  
569 free imaging of collective cell invasion and force-mediated deformations in collagen. *Scientific*  
570 *Reports*. 2021/02/02 2021;11(1):2814. doi:10.1038/s41598-021-81470-7

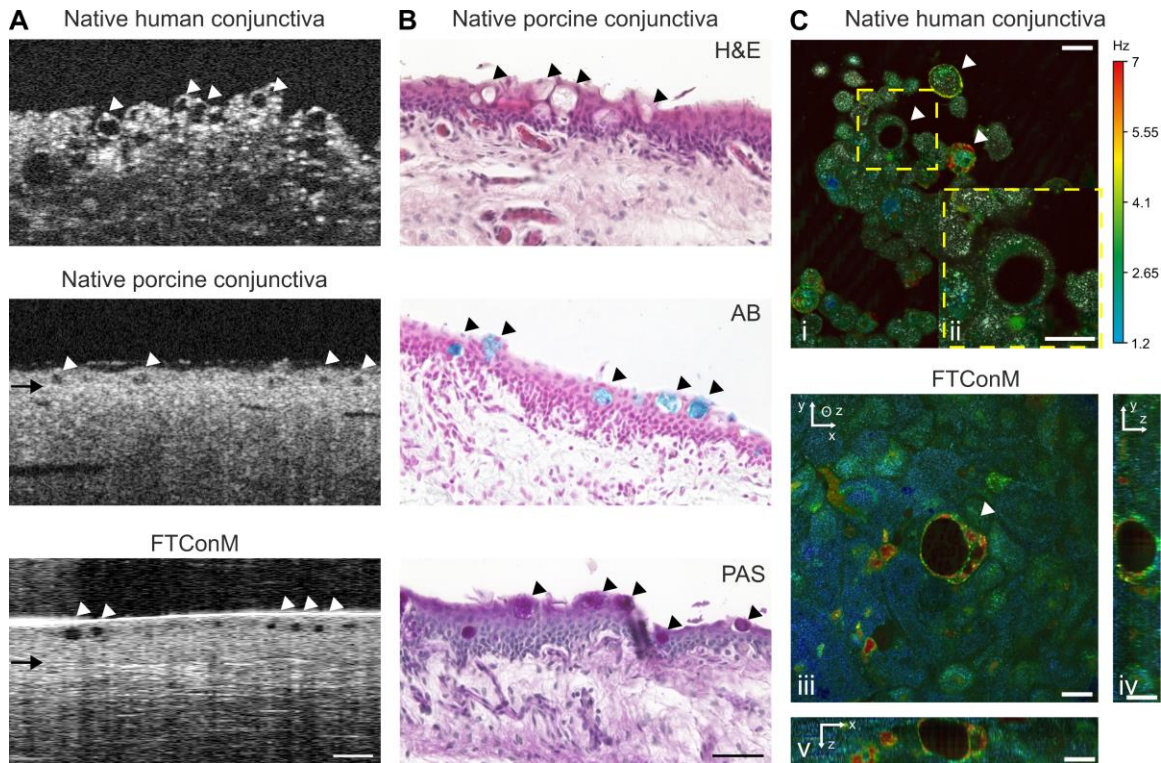
- 571 20. Haga K, Kamimura Y, Yamazaki M, et al. Quantitative and longitudinal monitoring of cancer  
572 cell invasion in a three-dimensional *in vitro* model of oral cancer using optical coherence  
573 tomography. *Sci Rep*. Nov 27 2025;doi:10.1038/s41598-025-28471-y  
574 21. Groux K, Verschuere A, Nanteau C, et al. Dynamic full-field optical coherence tomography  
575 allows live imaging of retinal pigment epithelium stress model. *Communications Biology*.  
576 2022/06/10 2022;5(1):575. doi:10.1038/s42003-022-03479-6  
577 22. Monfort T, Azzollini S, Brogard J, et al. Dynamic full-field optical coherence tomography  
578 module adapted to commercial microscopes allows longitudinal *in vitro* cell culture study.  
579 *Communications Biology*. 2023/09/28 2023;6(1):992. doi:10.1038/s42003-023-05378-w  
580 23. Apelian C, Harms F, Thouvenin O, Boccara AC. Dynamic full field optical coherence  
581 tomography: subcellular metabolic contrast revealed in tissues by interferometric signals temporal  
582 analysis. *Biomed Opt Express*. 2016/04/01 2016;7(4):1511-1524. doi:10.1364/BOE.7.001511  
583 24. Scholler J, Groux K, Goureau O, et al. Dynamic full-field optical coherence tomography: 3D  
584 live-imaging of retinal organoids. *Light: Science & Applications*. 2020/08/17 2020;9(1):140.  
585 doi:10.1038/s41377-020-00375-8  
586 25. Scholler J, Mazlin V, Thouvenin O, et al. Probing dynamic processes in the eye at multiple  
587 spatial and temporal scales with multimodal full field OCT. *Biomed Opt Express*. 2019/02/01  
588 2019;10(2):731-746. doi:10.1364/BOE.10.000731  
589 26. Thouvenin O, Boccara C, Fink M, Sahel J, Pâques M, Grieve K. Cell Motility as Contrast  
590 Agent in Retinal Explant Imaging With Full-Field Optical Coherence Tomography. *Investigative*  
591 *Ophthalmology & Visual Science*. 2017;58(11):4605-4615. doi:10.1167/iovs.17-22375  
592 27. Masuda Y, Hasebe R, Kuromi Y, Hishinuma M, Ohbayashi T, Nishimura R. Hatchability  
593 evaluation of bovine IVF embryos using OCT-based 3D image analysis. *J Reprod Dev*. Oct 20  
594 2023;69(5):239-245. doi:10.1262/jrd.2023-009  
595 28. Nithya S, Radhika T, Jeddy N. Loricrin - an overview. *J Oral Maxillofac Pathol*. Jan-Apr  
596 2015;19(1):64-8. doi:10.4103/0973-029x.157204  
597 29. Niiya A, Matsumoto Y, Ishibashi T, Matsumoto K, Kinoshita S. Collagen gel-embedding  
598 culture of conjunctival epithelial cells. *Graefes Arch Clin Exp Ophthalmol*. Jan 1997;235(1):32-40.  
599 doi:10.1007/bf01007835  
600 30. Lee DY, Lee SY, Yun SH, et al. Review of the Current Research on Fetal Bovine Serum and  
601 the Development of Cultured Meat. *Food Sci Anim Resour*. Sep 2022;42(5):775-799.  
602 doi:10.5851/kosfa.2022.e46  
603 31. Edin NF. The role of interleukin-13 in the removal of hyper-radiosensitivity by priming  
604 irradiation. *J Radiat Res*. Nov 2014;55(6):1066-74. doi:10.1093/jrr/rru053  
605 32. Hansen PM, Tollenaere MAX, Hedengran A, et al. IL-4 and IL-13 both contribute to the  
606 homeostasis of human conjunctival goblet cells *in vitro*. *Allergy*. Aug 2022;77(8):2555-2558.  
607 doi:10.1111/all.15326  
608 33. Kanoh S, Tanabe T, Rubin BK. IL-13-induced MUC5AC production and goblet cell  
609 differentiation is steroid resistant in human airway cells. *Clin Exp Allergy*. Dec 2011;41(12):1747-  
610 56. doi:10.1111/j.1365-2222.2011.03852.x  
611 34. Shi R, Jin M, Jin J, et al. Retinoic acid promotes conjunctival epithelium differentiation and  
612 goblet cell regeneration: evidence from novel 3D conjunctival organoids and whole-mount PAS  
613 staining. *Ocul Surf*. Jul 2025;37:301-313. doi:10.1016/j.jtos.2025.05.006  
614 35. Tanabe T, Fujimoto K, Yasuo M, et al. Modulation of mucus production by interleukin-13  
615 receptor alpha2 in the human airway epithelium. *Clin Exp Allergy*. Jan 2008;38(1):122-34.  
616 doi:10.1111/j.1365-2222.2007.02871.x  
617 36. Peștean C, Pavel A, Piciu D. Clinical and Paraclinical Considerations Regarding ki67's Role  
618 in the Management of Differentiated Thyroid Carcinoma—A Literature Review. *Medicina*.  
619 2024;60(5):769.  
620 37. Zhou H, Lu Q, Guo Q, et al. Vitriified collagen-based conjunctival equivalent for ocular surface  
621 reconstruction. *Biomaterials*. 2014;35(26):7398-7406.  
622 38. Jiang C, Centonze A, Song Y, et al. Collagen signaling and matrix stiffness regulate  
623 multipotency in glandular epithelial stem cells in mice. *Nature Communications*. 2024/12/18  
624 2024;15(1):10482. doi:10.1038/s41467-024-54843-5

- 625 39. Makuloluwa AK, Hamill KJ, Rauz S, et al. The conjunctival extracellular matrix, related  
626 disorders and development of substrates for conjunctival restoration. *The Ocular Surface*.  
627 2023;28:322-335.
- 628 40. He S, Huang Y, Dong S, et al. MiR-199a-3p/5p participated in TGF- $\beta$  and EGF induced EMT  
629 by targeting DUSP5/MAP3K11 in pterygium. *Journal of Translational Medicine*. 2020/09/01  
630 2020;18(1):332. doi:10.1186/s12967-020-02499-2
- 631 41. Malm SW, Amouzougan EA, Klimecki WT. Fetal bovine serum induces sustained, but  
632 reversible, epithelial-mesenchymal transition in the BEAS-2B cell line. *Toxicol In vitro*. Aug  
633 2018;50:383-390. doi:10.1016/j.tiv.2018.04.008
- 634 42. Finch PW, Rubin JS, Miki T, Ron D, Aaronson SA. Human KGF is FGF-related with  
635 properties of a paracrine effector of epithelial cell growth. *Science*. Aug 18 1989;245(4919):752-5.  
636 doi:10.1126/science.2475908
- 637 43. Komi-Kuramochi A, Kawano M, Oda Y, et al. Expression of fibroblast growth factors and their  
638 receptors during full-thickness skin wound healing in young and aged mice. *J Endocrinol*. Aug  
639 2005;186(2):273-89. doi:10.1677/joe.1.06055
- 640 44. Thomson AA, Cunha GR. Prostatic growth and development are regulated by FGF10.  
641 *Development*. Aug 1999;126(16):3693-701. doi:10.1242/dev.126.16.3693
- 642 45. Yun YR, Won JE, Jeon E, et al. Fibroblast growth factors: biology, function, and application  
643 for tissue regeneration. *J Tissue Eng*. Nov 7 2010;2010:218142. doi:10.4061/2010/218142
- 644 46. Babaei B, Davarian A, Lee SL, et al. Remodeling by fibroblasts alters the rate-dependent  
645 mechanical properties of collagen. *Acta Biomater*. Jun 2016;37:28-37.  
646 doi:10.1016/j.actbio.2016.03.034
- 647 47. Cialdai F, Risaliti C, Monici M. Role of fibroblasts in wound healing and tissue remodeling on  
648 Earth and in space. Review. *Frontiers in Bioengineering and Biotechnology*. 2022-October-04  
649 2022;Volume 10 - 2022doi:10.3389/fbioe.2022.958381
- 650 48. Coelho NM, Salmerón-Sánchez M, Altankov G. Fibroblasts remodeling of type IV collagen at  
651 a biomaterials interface. 10.1039/C3BM00163F. *Biomaterials Science*. 2013;1(5):494-502.  
652 doi:10.1039/C3BM00163F
- 653 49. Tamariz E, Grinnell F. Modulation of fibroblast morphology and adhesion during collagen  
654 matrix remodeling. *Mol Biol Cell*. Nov 2002;13(11):3915-29. doi:10.1091/mbc.e02-05-0291
- 655 50. Bell E, Ivarsson B, Merrill C. Production of a tissue-like structure by contraction of collagen  
656 lattices by human fibroblasts of different proliferative potential *in vitro*. *Proc Natl Acad Sci U S A*.  
657 Mar 1979;76(3):1274-8. doi:10.1073/pnas.76.3.1274
- 658 51. Boudko SP, Danylevych N, Hudson BG, Pedchenko VK. Basement membrane collagen IV:  
659 Isolation of functional domains. *Methods Cell Biol*. 2018;143:171-185.  
660 doi:10.1016/bs.mcb.2017.08.010
- 661 52. Messmer EM, Valet VM, Kampik A. Differences in basement membrane zone components of  
662 normal conjunctiva, conjunctiva in glaucoma and normal skin. *Acta Ophthalmol*. Sep  
663 2012;90(6):e476-81. doi:10.1111/j.1755-3768.2012.02481.x
- 664 53. Narayanan AS, Page RC, Swanson J. Collagen synthesis by human fibroblasts. Regulation  
665 by transforming growth factor-beta in the presence of other inflammatory mediators. *Biochem J*.  
666 Jun 1 1989;260(2):463-9. doi:10.1042/bj2600463
- 667 54. Massaro A, Villegas Novoa C, Wang Y, Allbritton NL. Fibroblasts modulate epithelial cell  
668 behavior within the proliferative niche and differentiated cell zone within a human colonic crypt  
669 model. Original Research. *Frontiers in Bioengineering and Biotechnology*. 2024-December-16  
670 2024;Volume 12 - 2024doi:10.3389/fbioe.2024.1506976
- 671 55. Iwashita J, Maeda H, Ishimura M, Murata J. Type IV collagen reduces MUC5AC secretion in  
672 the lungs of ovalbumin-sensitized mice. Original Research. *Frontiers in Pharmacology*. 2022-  
673 September-16 2022;Volume 13 - 2022doi:10.3389/fphar.2022.851374
- 674 56. Iwashita J, Yamamoto T, Sasaki Y, Abe T. MUC5AC production is downregulated in NCI-  
675 H292 lung cancer cells cultured on type-IV collagen. *Molecular and cellular biochemistry*.  
676 2010;337(1):65-75.

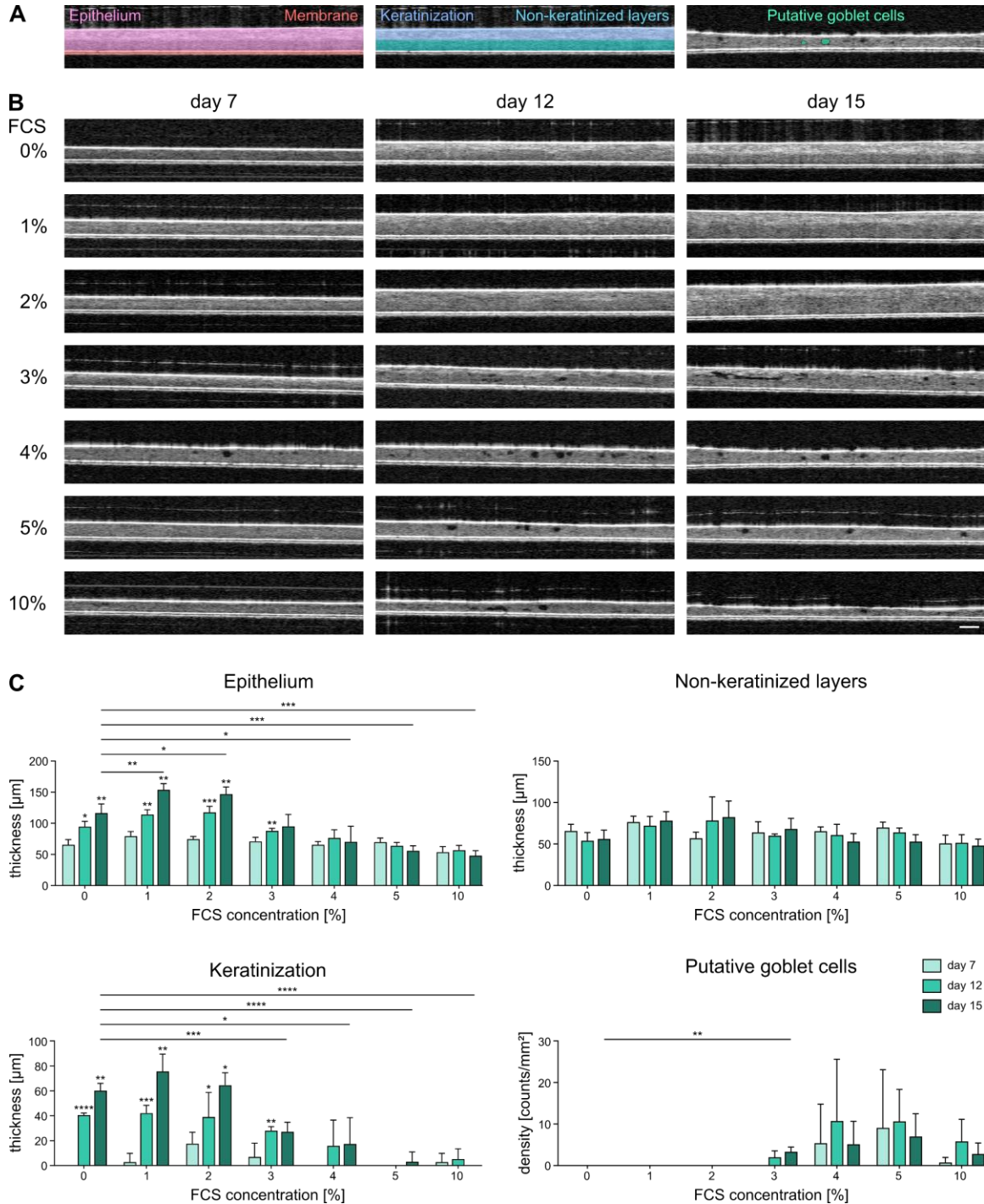
- 677 57. Zeppieri M, Marsili S, Enaholo ES, et al. Optical Coherence Tomography (OCT): A Brief Look  
678 at the Uses and Technological Evolution of Ophthalmology. *Medicina (Kaunas)*. Dec 3  
679 2023;59(12)doi:10.3390/medicina59122114
- 680 58. Sanchez MM, Orneles DN, Park BH, Morgan JT. Automated Epidermal Thickness  
681 Quantification of *in vitro* Human Skin Equivalents Using Optical Coherence Tomography.  
682 *BioTechniques*. 2022/05/01 2022;72(5):194-200. doi:10.2144/btn-2021-0123
- 683 59. Suebsamarn O, Kamimura Y, Suzuki A, et al. In-process monitoring of a tissue-engineered  
684 oral mucosa fabricated on a micropatterned collagen scaffold: use of optical coherence  
685 tomography for quality control. *Heliyon*. 2022/11/01/ 2022;8(11):e11468.  
686 doi:<https://doi.org/10.1016/j.heliyon.2022.e11468>
- 687 60. Aguirre A, Chen Y, Bryan B, et al. Cellular resolution *ex vivo* imaging of gastrointestinal  
688 tissues with optical coherence microscopy. *Journal of Biomedical Optics*. 2010;15(1):016025.
- 689 61. Kohlfærber T, Pieper M, MÜNter M, et al. Dynamic microscopic optical coherence tomography  
690 to visualize the morphological and functional micro-anatomy of the airways. *Biomed Opt Express*.  
691 Jun 1 2022;13(6):3211-3223. doi:10.1364/boe.456104
- 692 62. Kim J, Lee J, Kim S, et al. Noninvasive Imaging of Conjunctival Goblet Cells as a Method for  
693 Diagnosing Dry Eye Disease in an Experimental Mouse Model. *Translational Vision Science &*  
694 *Technology*. 2023;12(12):22-22. doi:10.1167/tvst.12.12.22
- 695 63. Portal C, Gouyer V, Gottrand F, Desseyn JL. Ocular mucins in dry eye disease. *Exp Eye Res*.  
696 Sep 2019;186:107724. doi:10.1016/j.exer.2019.107724
- 697 64. Tariq F. Allergic Conjunctivitis: Review of Current Types, Treatments, and Trends. *Life*  
698 *(Basel)*. May 21 2024;14(6)doi:10.3390/life14060650

699

700 **FIGURES AND TABLES**  
701

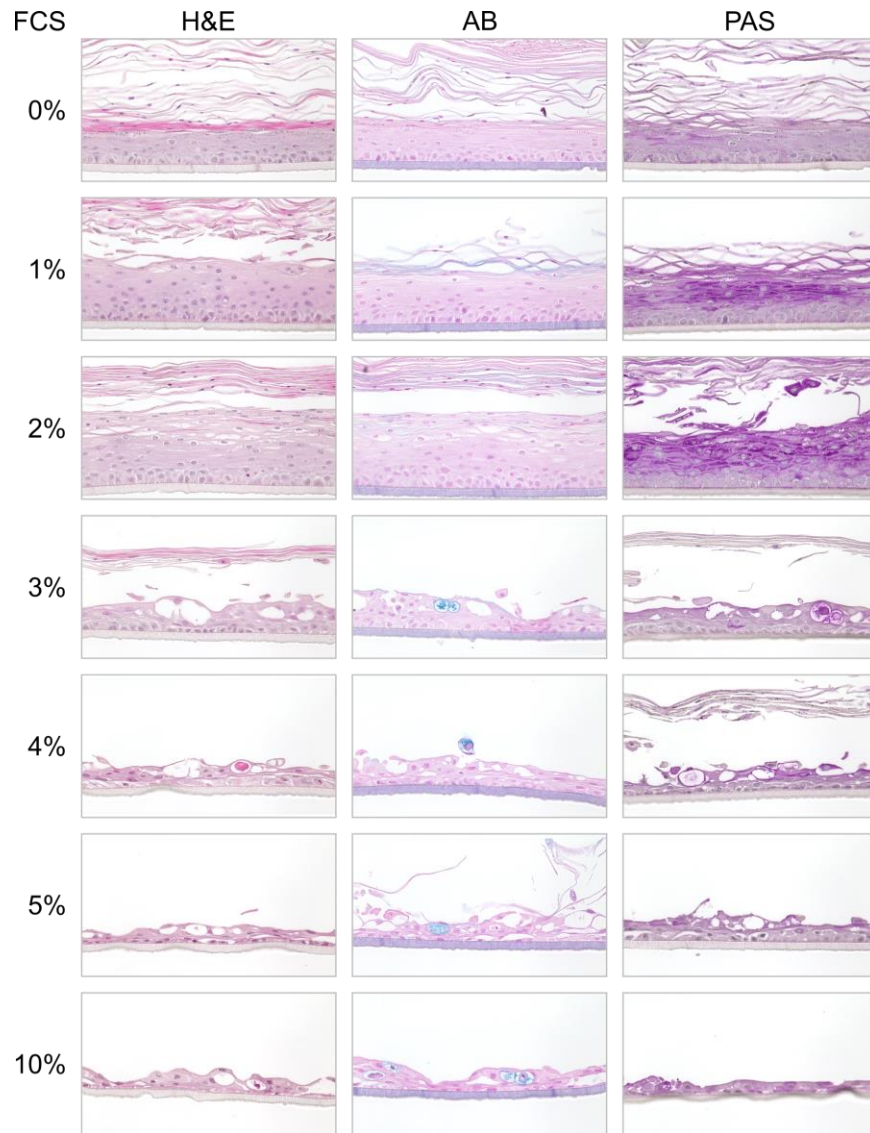


702 **Figure 1.** Comparison to *ex vivo* tissue verifies OCT as an adequate method to non-invasively  
703 detect epithelial architecture and goblet cells in 3D conjunctival *in vitro* models. **A** OCT imaging of  
704 native human and porcine conjunctiva and a FTConM, w/ Fib., 3% FCS. Scale bar:100  $\mu$ m. Black  
705 arrows indicate the transition from epithelium to stroma. **B** Hematoxylin&Eosin (H&E), Alcian blue  
706 (AB), and Periodic Acid Schiff (PAS) staining of native porcine conjunctiva. Scale bar: 50  $\mu$ m. **C**  
707 Dynamic full-field OCT (dFFOCT) z-stack of a native human conjunctiva (i, ii) and a FTConM (iii,  
708 iv, v) with an axial step of 10  $\mu$ m for native conjunctiva and 1  $\mu$ m for FTConM. Hue scales from 1.2  
709 to 7 Hz mean frequency. **i** A selected XY cross-section of native conjunctiva. **ii** zoom-in on (i),  
710 indicated by the yellow square, is displayed in (ii), where a goblet cell can be distinguished. **iii** An  
711 en face (XY) cross-section from within the FTConM, at 17  $\mu$ m depth. **iv** A reconstructed YZ cross-  
712 section from within the FTConM, using 31 en face images with an axial step of 1  $\mu$ m. **v** A  
713 reconstructed XZ cross-section from within the FTConM, using the same en face images as in (iv).  
714 Scale bars:20  $\mu$ m. Goblet cells are indicated by arrowheads.  
715  
716  
717  
718



719  
720  
721  
722  
723  
724  
725  
726  
727

**Figure 2.** Optical Coherence Tomography (OCT) analysis of rhConE cultured with increasing FCS concentrations. **A** Schematic example of how tissue parameters were analyzed from OCT images. **B** OCT images from day 7, 12 and 15 of rhConE cultured with 0 – 10% FCS. Scale bar: 100  $\mu\text{m}$ . **C** Quantitative analysis of total epithelial thickness, non-keratinized layers, keratinization and goblet cell density of rhConE using OCT 3D stacks and Imaris software ( $n = 6$ ). Mean + SD; \* $p < 0.05$ , \*\* $p < 0.01$ , \*\*\* $p < 0.001$ , \*\*\*\* $p < 0.0001$ .



728  
729  
730  
731  
732  
733  
734

**Figure 3.** Dose-dependent effects of FCS on the epithelial stratification and presence of mucus-containing cells in rhConE. Hematoxylin&Eosin (H&E), Alcian blue (AB), and Periodic Acid Schiff (PAS) staining of rhConE supplemented with 0 – 10% FCS. Models were stained at day 15 of culture. Scale bar: 50  $\mu$ m.

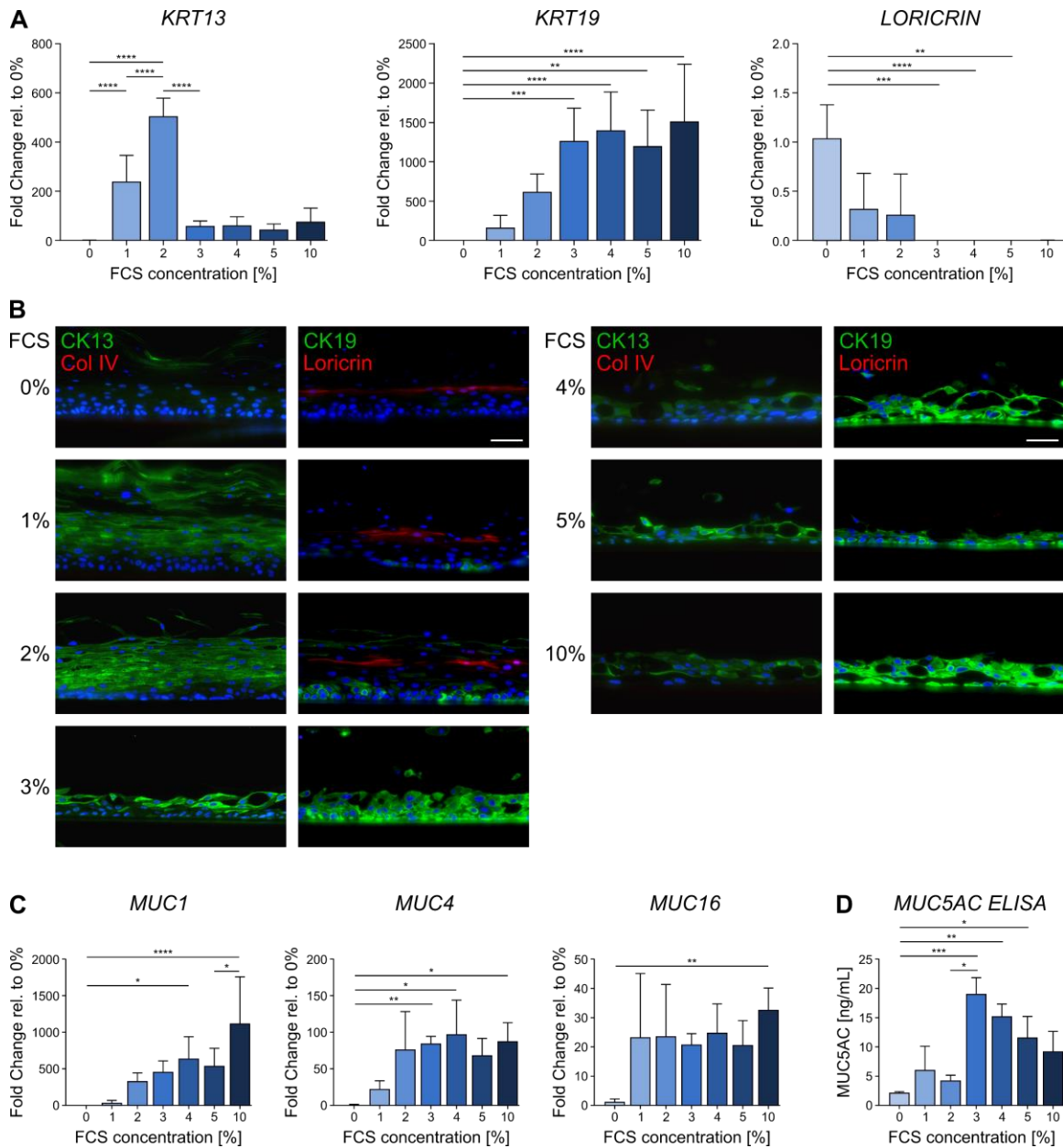
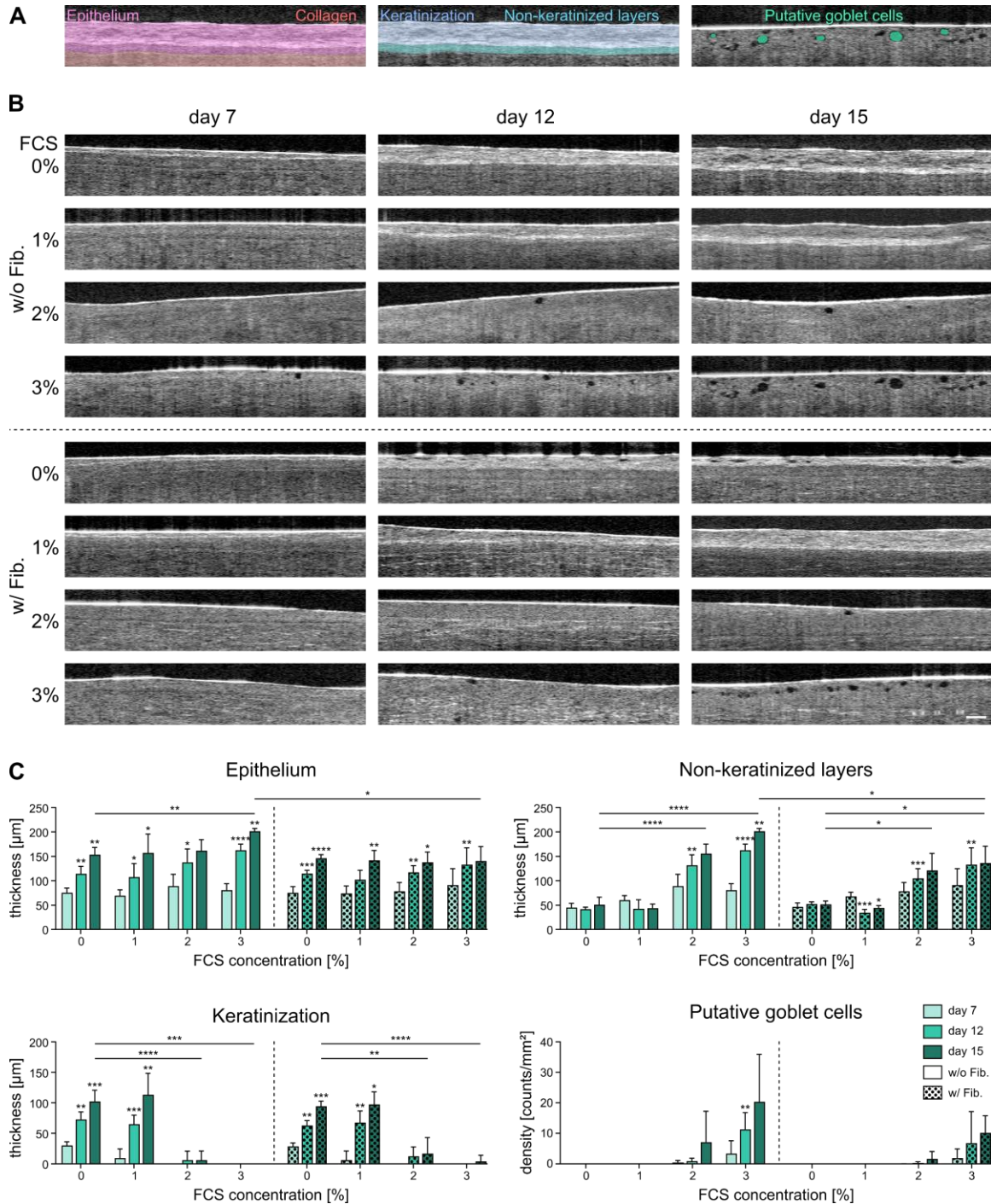


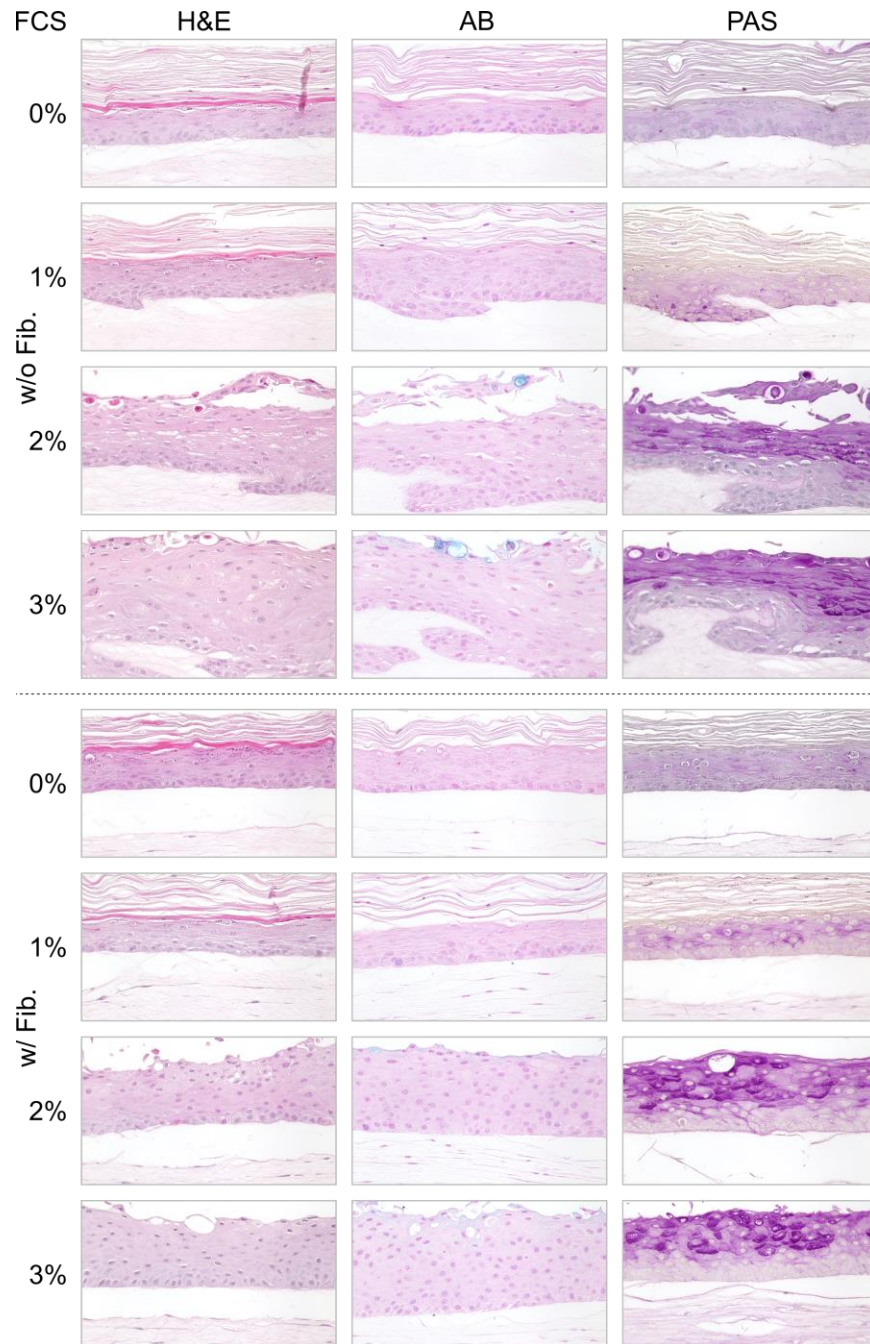
**Figure 4.** Analysis of specific marker expression in rhConE cultured with FCS concentrations of 0 – 10%. **A** RT-qPCR of KRT13, KRT19, and LORICRIN (n = 3). **B** Immunofluorescence of CK13, CK19, Loricrin, and Col IV. DAPI = blue. Scale bar: 50  $\mu$ m. **C** RT-qPCR of membrane-associated mucins MUC1, MUC4, and MUC16 (n = 3). **D** ELISA of secreted MUC5AC (n = 3). Mean + SD; \*p < 0.05, \*\*p < 0.01, \*\*\*p < 0.001, \*\*\*\*p < 0.0001.

735  
736  
737  
738  
739  
740  
741  
742  
743



744  
745  
746  
747  
748  
749  
750  
751  
752

**Figure 5.** OCT analysis of FTConM cultured without (w/o Fib.) and with (w/ Fib.) fibroblasts and increasing FCS concentrations. **A** Schematic example of how tissue parameters were analyzed from OCT images. **B** OCT images from day 7, 12 and 15 of FTConM cultured with 0 – 3% FCS. Scale bar:100 μm. **C** Quantitative analysis of total epithelial thickness, non-keratinized layers, keratinization and goblet cell density of FTConM using Imaris software (n = 6). Mean + SD; \*p < 0.05, \*\*p < 0.01, \*\*\*p < 0.001, \*\*\*\*p < 0.0001.



753  
754  
755  
756  
757  
758  
759  
760  
761

**Figure 6.** Effects of varying FCS concentrations in FTConM with and without fibroblasts on epithelial stratification and the occurrence of mucus-containing cells. Hematoxylin&Eosin (H&E), Alcian blue (AB), and Periodic Acid Schiff (PAS) staining of FTConM without (w/o Fib.) and with (w/ Fib.) fibroblasts, supplemented with 0 – 3% FCS. Models were stained on day 15 of culture. Scale bar: 50 μm.

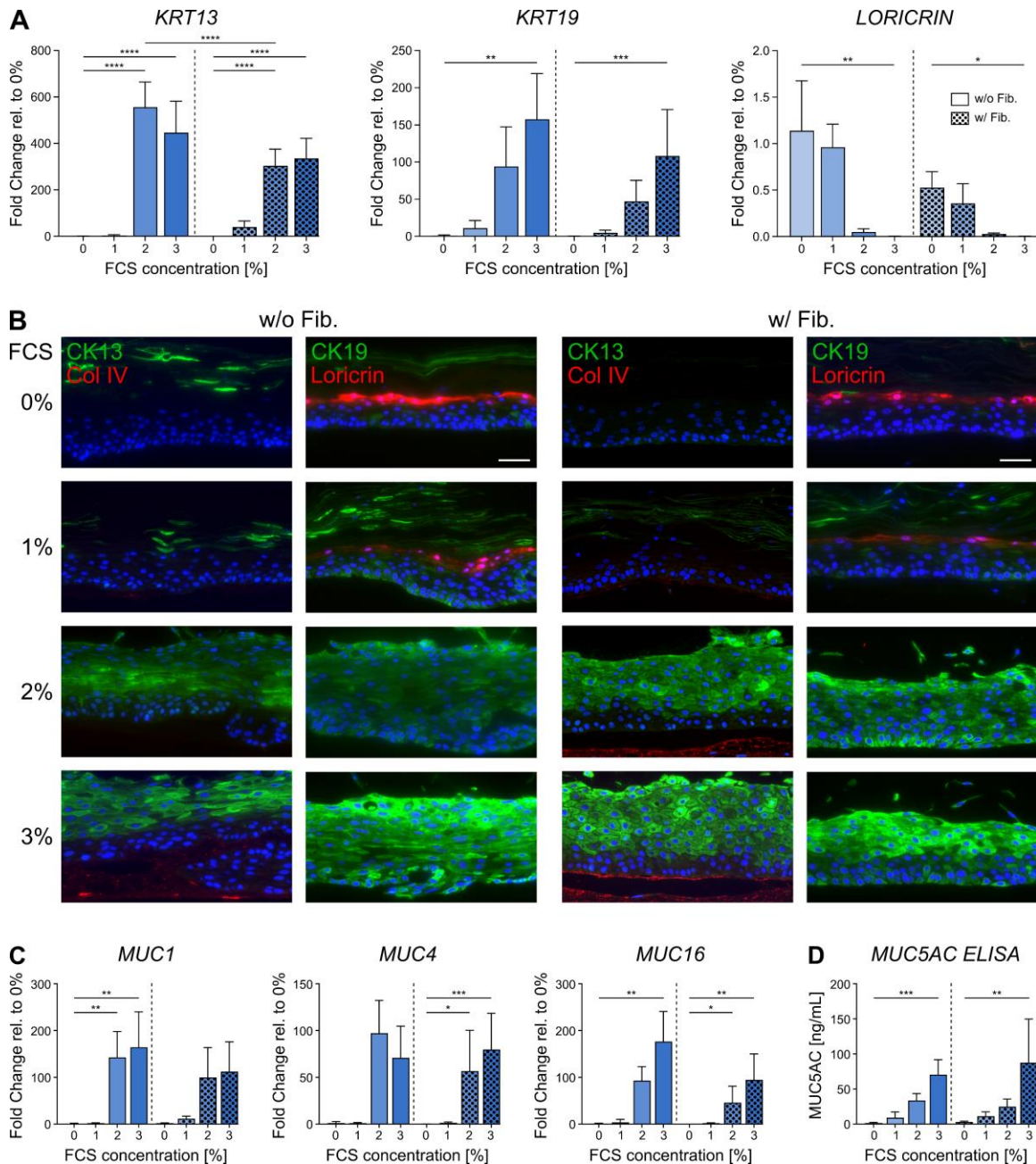


**Figure 7.** Analysis of specific marker expression in FTConM cultured with FCS concentrations of 0 – 3%. **A** RT-qPCR of KRT13, KRT19, and LORICRIN ( $n = 3$ ). **B** Immunofluorescence of Cytokeratin (CK) 13, CK19, Loricrin, and Col IV. DAPI = blue. Scale bar: 50  $\mu\text{m}$ . **C** RT-qPCR of membrane-associated mucins MUC1, MUC4, and MUC16 ( $n = 3$ ). **D** ELISA of secreted MUC5AC ( $n = 3$ ). Mean + SD; \* $p < 0.05$ , \*\* $p < 0.01$ , \*\*\* $p < 0.001$ , \*\*\*\* $p < 0.0001$ .

762  
763  
764  
765  
766  
767  
768  
769  
770

771 **Table 1.** Primers used for RT-qPCR  
772

Gene	Gene Function	Primer sequence (5' - 3')	
<i>18s</i>	Housekeeping	F	CTCAACACGGGAAACCTCAC
		R	CGCTCCACCAACTAAGAACG
<i>KRT13</i>	Cytokeratin	F	TGAGATGGAGTGCCAGAACC
		R	AAGGGAAACCAATCATCTTGGC
<i>KRT19</i>	Cytokeratin	F	GCAGGTCCGAGGTTACTGAC
		R	CCAAGGCAGCTTTCATGCTC
<i>LORICRIN</i>	Cornified envelope	F	TTGGAGGTGTTTTCCAGGGG
		R	TGCAAACCTCGGGTAGCATC
<i>MUC1</i>	Membrane-associated mucin	F	TGTCAGTGCCGCCGAAAGAA
		R	CTACAAGTTGGCAGAAGTGG
<i>MUC4</i>	Membrane-associated mucin	F	GACTTGGAGCTCTTTGAGAATGG
		R	TGCAATGGCAGACCACAGTCC
<i>MUC16</i>	Membrane-associated mucin	F	GCCTCTACCTTAACGGTTACAATGAA
		R	GGTACCCCATGGCTGTTGTG

773  
774